



ELSEVIER

Available online at www.sciencedirect.com

SCIENCE @ DIRECT®

Nuclear Instruments and Methods in Physics Research B 207 (2003) 107–123

NIM B
Beam Interactions
with Materials & Atomswww.elsevier.com/locate/nimb

Experimental benchmarks of the Monte Carlo code PENELOPE

J. Sempau^{a,*}, J.M. Fernández-Varea^b, E. Acosta^c, F. Salvat^b^a *Institut de Tècniques Energètiques, Universitat Politècnica de Catalunya. Diagonal 647, 08028 Barcelona, Spain*^b *Facultat de Física (ECM), Universitat de Barcelona, Societat Catalana de Física (IEC), Diagonal 647, 08028 Barcelona, Spain*^c *Facultad de Matemática, Astronomía y Física, Universidad Nacional de Córdoba. Ciudad Universitaria, 5000 Córdoba, Argentina*

Received 1 August 2002; received in revised form 17 December 2002

Abstract

The physical algorithms implemented in the latest release of the general-purpose Monte Carlo code PENELOPE for the simulation of coupled electron–photon transport are briefly described. We discuss the mixed (class II) scheme used to transport intermediate- and high-energy electrons and positrons and, in particular, the approximations adopted to account for the energy dependence of the interaction cross-sections. The reliability of the simulation code, i.e. of the adopted interaction models and tracking algorithms, is analyzed by means of a comprehensive comparison of simulation results with experimental data available from the literature. The present analysis demonstrates that PENELOPE yields a consistent description of electron transport processes in the energy range from a few keV up to about 1 GeV.

© 2003 Elsevier Science B.V. All rights reserved.

PACS: 78.70.–g

Keywords: Radiation transport; Monte Carlo simulation; Electron–gamma showers

1. Introduction

The PENELOPE code system simulates the coupled transport of electrons, positrons and photons in complex geometries and arbitrary materials. Distributed through the NEA Data Bank,¹ the first version of this code was brought to light in 1996. A detailed description of its components and

capabilities can be found in previous publications [1–3]. A modification of the 1996 simulation package was developed during the year 2000 as an intermediate step towards the current 2001 version. For the sake of brevity, hereafter we shall use the name PENELOPE to refer to this latest version.

PENELOPE contains considerably improved electron interaction models and more elaborate tracking algorithms for mixed simulation of intermediate- and high-energy electron transport with respect to the 1996 version. These new tracking algorithms increase the stability of the code under variation of the simulation parameters (see below) and, as a consequence, they allow the simulation to be speeded up without sacrificing

* Corresponding author. Tel.: +34-93-4016074; fax: +34-93-4017149.

E-mail address: josep.sempau@upc.es (J. Sempau).

¹ OECD Nuclear Energy Agency Data Bank. Le Seine Saint-Germain, 12 Boulevard des Iles, 92130 Issy-les-Moulineaux, France (<http://www.nea.fr>).

accuracy. A detailed and practically oriented description of PENELOPE is given in a report by Salvat et al. [4], which is published and distributed with the code by the NEA. In the present article, only the most relevant changes in the physical models and simulation algorithm will be outlined; for a more detailed description the reader is referred to the publication [4].

Experimental results are always affected by the so-called type-B uncertainties,² which are often non-negligible and too frequently underestimated or unknown. When independent measurements of the same quantity are available from different laboratories (this is the case of electron backscattering coefficients, for example, see below), the dispersion among the results provides an indication of their reliability and the comparison of the whole experimental data set with simulation results allows more objective conclusions to be extracted about the reliability of the simulation. In other cases, where only a single experiment or multiple measurements performed at a single laboratory are available, comparison of experimental data with simulation results is less conclusive. The worst situations are found when the description of the experimental arrangement lacks essential details and when experimental data are not accurately represented. Unfortunately, for the sake of economy of space, many authors publish their experimental data in graphical form instead of giving them (and their uncertainties) numerically; then the plots need to be digitized (after being scanned or photocopied), a process that may easily introduce additional systematic errors. Bearing all this in mind, our main objective here is to present a broad spectrum of experiments against which the models and algorithms of PENELOPE can be validated.

This article is organized as follows. In Section 2 we summarize the most relevant elements of the simulation code. Sections 3–5 are devoted to the

physical models and tracking algorithms. In Section 6, which constitutes the central part of the present work, we focus on the results and analysis of the extensive set of benchmarks intended to test and validate the PENELOPE code and, especially, the bremsstrahlung model. Finally, in Section 7 some conclusions are drawn.

2. The simulation package

PENELOPE generates electron–photon showers produced by primary particles (electrons, photons or positrons) in matter. The code operates within the energy range from 100 eV up to 1 GeV and for homogeneous materials with arbitrary compositions (involving elements with atomic number $Z = 1–92$). Compound materials and mixtures are described by means of the additivity approximation, i.e. the cross-section (CS) of a molecule is the sum of atomic CSs of the different atoms in the molecule. The core of the code is a set of FORTRAN 77 subroutines which are invoked from a simple steering main program, to be provided by the user. PENELOPE does most of the simulation work internally and little knowledge of the physics involved in the transport process is required from the user.

The code system contains a geometry package called PENGEOM that does automatic tracking of particles within quadric geometries, i.e. within any set of homogeneous material volumes limited by quadric surfaces. It includes programs for displaying two- and three-dimensional pictures of the geometry, GVIEW2D and GVIEW3D. These two programs, which run on MS-Windows 9x and NT systems, are essential tools for writing and debugging geometry definition files.

The distribution package also contains several examples of main programs. Among them, PENSLAB.F simulates transport of radiation in a homogeneous slab and PENCYL.F does simulation in cylindrical geometries. These two codes provide very detailed simulation results (covering virtually all measurable quantities) and can be used to reproduce most of the simulation results presented in Section 6. The package PENFIELD.F, also included, allows the simulation of electron and

² See [5] for a detailed description of this terminology. Hereafter and when referring to Monte Carlo calculations, we shall use the expression “statistical uncertainty” to denote type-A uncertainties. Notice that, somewhat imprecisely, type-B uncertainties were formerly termed “systematic”.

positron transport in the presence of static external magnetic and electric fields of relatively moderate intensity.

3. Photon transport

The transport of photons is treated in the conventional detailed way, i.e. by simulating all interactions along a photon history in chronological succession. The considered interaction mechanisms are coherent (Rayleigh) scattering, incoherent (Compton) scattering, pair (and triplet) production and photoelectric absorption. For a detailed description of the physical models and simulation algorithms of the first three of these mechanisms see [6] and [7].

The description of photoelectric absorption has recently been modified to enable the simulation of X-ray and Auger electron emission from vacancies in K and L electron shells (hereafter, these will be referred to as inner shells). PENELOPE makes use of photoelectric total atomic CSs and partial CSs for the K, L1, L2 and L3 shells to determine the shell of the active electron, from which the subsequent atomic relaxation cascade will start. These photoelectric CSs have been extracted, in the form of numerical tables, from the LLNL Evaluated Photon Data Library (EPDL) and are based on the first-order multipole calculations by Scofield [8]. These tables cover the elements $Z = 1-92$ for a grid of energies dense enough to ensure that linear log–log interpolation is accurate to within 1%.

After absorption of a photon by an inner shell, the de-excitation cascade of the ionized atom is followed until all vacancies have migrated to M and outer shells. The corresponding transition probabilities and energies have been extracted from the LLNL Evaluated Atomic Data Library (EADL) [9].

4. Electron interactions

4.1. Elastic scattering

Elastic scattering of electrons and positrons is described by means of the total CS and the first

and second transport CSs obtained from Dirac partial-wave calculations [10]. The mean free path, used to determine the location of elastic scattering events, is evaluated from the total CS. The distribution of angular deflections in each individual event is modelled as a statistical admixture of a Wentzel distribution (that corresponds to scattering by an exponentially screened Rutherford potential within the first Born approximation), a fixed-angle distribution and a triangular distribution. The relative weights of these three components are set in such a way that the first and second moments of the single-scattering angular distribution obtained by partial-wave analysis are exactly reproduced. This “modified” Wentzel model differs slightly from the W2D model used in the 1996 version of PENELOPE and yields improved large-angle angular distributions in the plural scattering regime (i.e. for a few interactions).

It should be noted that the single-scattering angular distribution used by PENELOPE differs from the “true” distribution (i.e. that obtained from the partial-wave calculations). However, its shape is physically plausible and its first and second moments are correct. This suffices to ensure reliable simulation results whenever the number of elastic events per electron track is “statistically sufficient” (in practice, larger than 10 or so) [11]. Moreover, the modified Wentzel model requires only a minimum of numerical information (three energy-dependent quantities) and allows the formulation of mixed simulation algorithms with ease. Notice also that the model consistently accounts for differences between elastic scattering of electrons and positrons.

4.2. Inelastic scattering

Inelastic collisions of electrons and positrons are treated in essentially the same way as in the 1996 version of PENELOPE. The simulation is based on the relativistic first Born approximation, with a generalized oscillator strength model initially proposed by Liljequist [12,13]. The response of each atomic shell is described by a so-called δ -oscillator with oscillator strength equal to the number of electrons in the shell and resonance energy chosen so as to reproduce the mean

ionization energy of the simulated material, the fundamental parameter of the model. Close collisions are described by means of the Møller and Bhabha CSs for collisions with free electrons at rest, which account for exchange and annihilation–recreation effects, respectively.

This model also allows a consistent description of the density effect (equivalent to that of Sternheimer [14]) and gives collision stopping powers in close agreement with those from the ICRU 37 tables [15]. Furthermore, it yields analytical expressions for the differential CS (differential in the energy loss and the scattering angle) of electrons and positrons from which the simulation of inelastic events can be performed by using analytical sampling methods. The model is well suited for mixed simulations, because it permits exact simulation of hard collisions and gives analytical expressions for the various moments of the (restricted) energy loss and the angular deflection in soft inelastic events.

It is important to note that, although the model introduced above is adequate to provide an accurate representation of the transport of the projectile, the description of inner-shell ionizations produced by electron impact is too simplistic and may therefore lead to substantial discrepancies with experimental results related to this effect. We are currently developing a new model that overcomes these limitations by incorporating inner-shell ionization CSs by electron impact calculated from the distorted-wave Born approximation [16], a theoretical approach whose accuracy has been proved by direct comparison with measurements [17]. These improvements will be made available in future releases of the code.

4.3. Bremsstrahlung emission

Radiative interactions, in which an electron or positron of initial kinetic energy E radiates a photon of energy W in a direction forming an angle θ with the initial direction of the projectile, are described by a CS differential in W , θ and the angular deflection of the projectile [18,19]. A first simplification, adopted in all simulation codes currently available, is to assume that angular deflections of the projectile are accounted for by the

elastic scattering CS and, consequently, the direction of movement of the projectile is kept unaltered in radiative events. For isotropic media with randomly oriented atoms or molecules, the bremsstrahlung differential CS can be expressed as

$$\frac{d^2\sigma}{dW d(\cos\theta)} = \frac{Z^2}{\beta^2} \frac{1}{W} \chi(Z, E, W) p(Z, E, W; \cos\theta), \quad (1)$$

where β is the velocity of the projectile in units of the speed of light, Z is the atomic number of the target and $p(Z, E, W; \cos\theta)$ is the probability distribution function (PDF) of $\cos\theta$ (normalized to unity), the so-called shape function. The product $W^{-1}\chi$ is the (unnormalized) PDF of the energy loss W in each radiative event; the function $\chi(Z, E, W)$ is known as the scaled bremsstrahlung differential CS. Seltzer and Berger [20,21] have produced extensive tables of the scaled differential CS for all the elements and energies from 1 keV to 10 GeV by combining various theoretical calculations. On the other hand, Kissel et al. [22] published numerical tables of the shape function for selected values of Z , E and W calculated by partial-wave methods. These data constitute the most reliable theoretical representation of the bremsstrahlung energy spectra and angular distributions available at present.

Since the tabulation of $d^2\sigma/dW d(\cos\theta)$ on a dense enough grid to permit accurate numerical interpolation would require a considerable amount of computer memory, the habitual practice in Monte Carlo simulation codes is to sample the energy loss W from the single-variate distribution obtained by integrating Eq. (1) over $\cos\theta$. For a given element Z , the scaled differential CS varies smoothly with E and W and can therefore be interpolated with a modest amount of computer memory. This approach allows the sampling of W easily, but information on the angular distribution has to be regained from suitable approximations. This uncoupled scheme is adopted in many well-known codes, e.g. EGS4 [23], ITS3 [24], MCNP [25], etc.

In contrast, PENELOPE relies on a new method recently developed by Acosta et al. [26], which is based on an analytical approximation to the shape

function (a Lorentz-boosted dipole-like distribution). This approximation contains two adjustable parameters that are determined by least-squares fitting to Kissel et al.'s tabulated shape functions. It is found that the fit is very accurate and that the parameters vary smoothly with Z , E and W so that they can be readily obtained by interpolation. In PENELOPE, the simulation of each radiative event proceeds as follows. First, for the considered material Z and kinetic energy of the projectile E , the energy loss W is sampled from the corresponding PDF, determined by the scaled function $\chi(Z, E, W)$. Afterwards, the angle of emission of the photon is sampled according to the parameterized shape function $p(Z, E, W; \cos\theta)$ (the sampling is done analytically). This method accounts for the correlation between W and $\cos\theta$ in a rigorous way. Unfortunately, Kissel et al. tabulated the shape functions only over the energy interval between 1 and 500 keV and extrapolation to higher energies is unclear. For $E > 500$ keV, PENELOPE uses the classical Lorentz-boosted dipole angular distribution of photons, the same as in the 1996 version, which agrees with the dominant term obtained from high-energy Born calculations.

4.4. Positron annihilation

As in the 1996 version, the currently used algorithm relies on the differential CS given by Heitler [27] and transformed to the laboratory reference frame by Nelson et al. [23]. Within this scheme, positrons annihilate, either in-flight or at rest, with a free and motionless electron, thus binding and Doppler effects are disregarded.

5. Electron transport mechanics

The main differentiating feature of PENELOPE is the consistent use of mixed simulation, or class II simulation in Berger's terminology [28], to describe the transport of electrons and positrons. In mixed simulation, interactions are classified into "hard" and "soft" by defining suitable cutoff values for the energy loss and the angular deflection. Hard interactions involve energy transfers and/or angular deflections larger than the cutoff values and are

simulated individually. Soft interactions, with small energy transfers or small deflections, have a mild effect on the particle tracks. In the simulation of intermediate- and high-energy projectiles, where mixed simulation is helpful, a large average number of soft collisions occur between each pair of hard events and their combined effect can be simulated as a single artificial soft event using multiple scattering approaches.

In contrast to PENELOPE, most general-purpose codes either use pure condensed (class I) simulation or combine condensed schemes for elastic scattering with mixed simulation of energy-loss events. Both condensed and mixed simulation schemes produce a reduction in computing time by the mere fact that the number of events to be simulated is also reduced. Mixed simulation is superior, because of its better accuracy and robustness. The higher accuracy is expected a priori from the fact that hard collisions are described in an exact way – provided the differential CSs employed are correct. The robustness of mixed simulation arises from its stability with respect to changes in the simulation parameters and from the relative simplicity of the tracking algorithm (for details see [4]).

PENELOPE generates electron space displacements and determines the effect of soft energy loss and scattering mechanisms by using the random-hinge method, which was already implemented in the 1996 version. The current version, however, incorporates several improvements that give better stability and, consequently, allow acceleration of the simulation. Firstly, the PDFs for soft scattering and energy loss events have been modified to represent the true distributions more accurately, even under plural scattering conditions. Secondly, the tracking algorithm has been extended to account for the fact that the electron loses energy between each pair of consecutive hard events due to soft interactions. On the one hand, the algorithm takes the variation with energy of the differential CSs for soft interactions into consideration by assuming that they vary linearly with energy. On the other hand, the energy dependence of the inverse mean path of hard collisions, which is used to sample the distance to the next hard event, is taken into account *exactly* by means of a

trick borrowed from photon and neutron transport studies and known as the δ -scattering method [29]. The trick consists of considering a fictitious interaction mechanism that does nothing (delta interactions) and has an inverse mean free path that varies with energy in such a way that the total mean free path for the combined process (i.e. real interactions and delta scattering) remains constant in the energy range swept by the projectile along a step. The mean free path to the next interaction is sampled from the exponential distribution with this constant inverse mean free path; the occurrence of delta interactions compensates the energy dependence of the inverse mean free path of the actual hard events. Full details can be found in [4].

The user can tune the mixed simulation algorithm by defining the values of the following simulation parameters:

- C1: limits the average angular deflection of an electron along the track segment between two hard events. The following relation holds, $C1 \simeq 1 - \langle \cos \Theta \rangle$, where Θ denotes the multiple scattering polar deflection after a step of length equal to the mean free path between hard events. Notice that with a larger value of C1 we get a larger hard mean free path and, therefore, the simulation speeds up since there are fewer hard elastic events.
- C2: sets an upper bound to the average fractional energy loss of the projectile along the track segment between two hard events, $C2 \simeq \langle \Delta E \rangle / E$. This parameter has an effect only at energies for which bremsstrahlung emission becomes appreciable.
- WCC and WCR: cutoff energy losses for inelastic collisions and bremsstrahlung emission, respectively. These two parameters set the boundaries between soft and hard interactions. When they are increased the simulation speeds up. WCC is more effective at low energies, whereas the effect of WCR is appreciable only when radiative interactions dominate, i.e. at high energies.
- DSMAX: maximum allowed step length. When the distance to the next hard event is larger than DSMAX, PENELOPE sets the step length equal to DSMAX and simulates a delta interaction at the

end of the step. This parameter is useful for controlling the average number of soft events (hinges) undergone by an electron or positron in a thin medium – although it does not affect the average number of hard interactions. The simulation is reliable only when the average number of hinges along each electron or positron track is of the order of ten or larger.

(For a more detailed analysis of the role of these parameters, see [4].)

6. Results

The experiments and simulations presented in this section may be grouped into four categories, namely, (i) backscattering, transmission and absorption of electrons (or positrons) through material slabs (Figs. 1–8); (ii) depth and radial distributions of deposited energy (or absorbed doses) in homogeneous media (Figs. 9–11); (iii) thick-target bremsstrahlung spectra (Figs. 12–17); and (iv) coupling between photon and electron/positron transport (Fig. 18). Our main interest here is in electron transport because this is the problem that motivated most of the original features of PENELOPE. Thus, benchmarks in group (i) aim to probe the delicate balance between energy loss and angular deflection required to describe the energy-angular distributions of the electrons that emerge from the irradiated material slabs as well as the implantation profiles. In addition to these two mechanisms, some cases of group (ii) also explore the coupling between electron and photon transport. The experiments in group (iii) serve mostly to validate the model and sampling algorithm for bremsstrahlung emission and, to a lesser extent, the transport of the generated photons within the sample. Finally, the case presented in (iv) investigates the transport of the electrons and positrons generated by a high-energy photon beam.

The simulation parameters adopted in the different cases were set as follows. The absorption energy EABS for electrons and positrons, at which the simulation of these particles is discontinued, was set equal to 1% of the kinetic energy of the

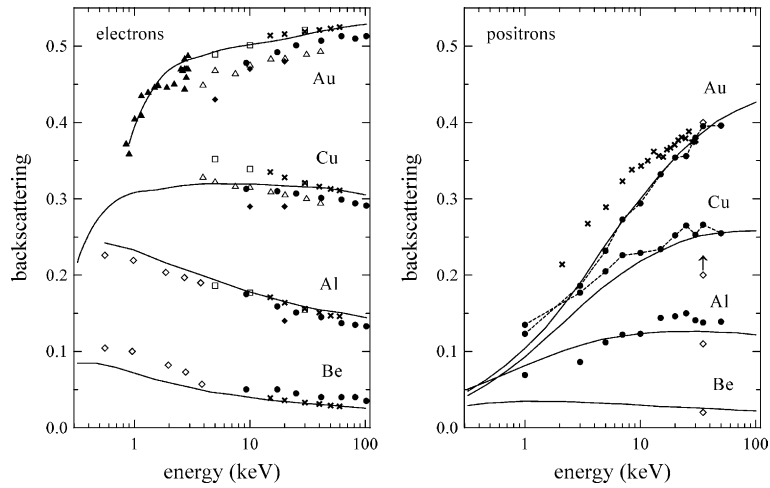


Fig. 1. Backscattering coefficients for electrons and positrons (at normal incidence) and bulk samples of various elements, as functions of the energy of the incident particles. Solid lines are results from PENELOPE. Symbols represent experimental data from the following references. For electrons: solid dots, [30]; crosses, [31]; hollow diamonds, [32]; hollow triangles, [33]; solid triangles, [34]; solid diamonds, [35]; hollow squares, [36] (quoted in [31]). For positrons: hollow diamonds, [37]; solid dots, [38]; crosses, [39].

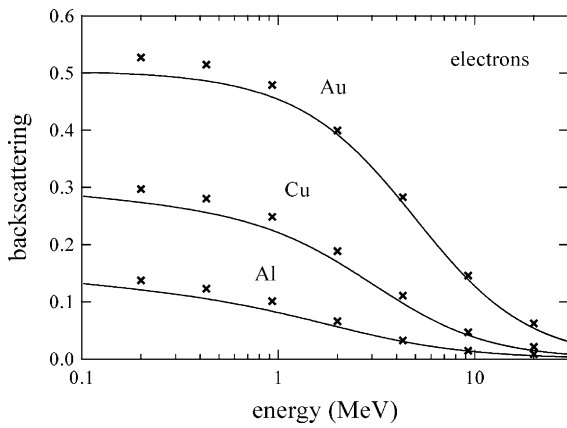


Fig. 2. Backscattered fractions from electron beams normally incident on different bulk samples as functions of the kinetic energy. Symbols are results from PENELOPE, with absolute uncertainties between 0.001 and 0.006. Lines represent the empirical equation from [40].

primary (source) particles – except for backscattering and transmission experiments, which are discussed below. For photons, we set $EABS(\gamma) = 0.1 \times EABS(e^-)$. In all cases WCC and WCR were taken equal to $EABS(e^-)$ and $EABS(\gamma)$, respectively. The parameters C1 and C2 were set equal to 0.05. Whenever thin layers were involved in the simulation, DSMAX was assigned a value equal to 1/10 of the corresponding layer thickness, so as to

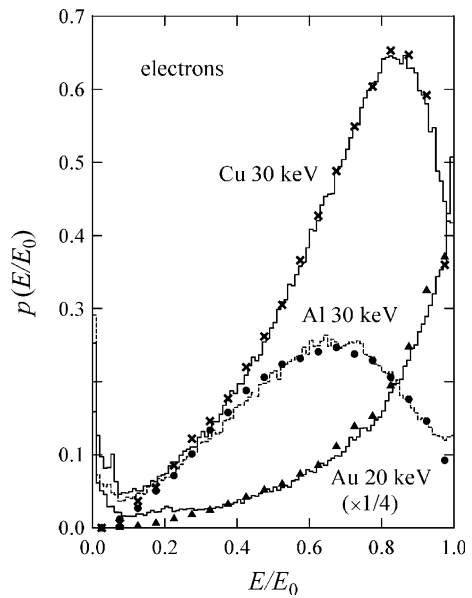


Fig. 3. PDF of backscattered electrons impinging normally on different bulk samples. The beam energy E_0 and composition are indicated for each case. PENELOPE's results are represented as histograms. Experimental data, represented by symbols, are from Darlington [42], who renormalized them to the bulk-backscattering fractions from [30]. Notice the scaling of the gold curve for clarity.

ensure that at least there are, on average, ~ 10 hinges along each electron track. Otherwise,

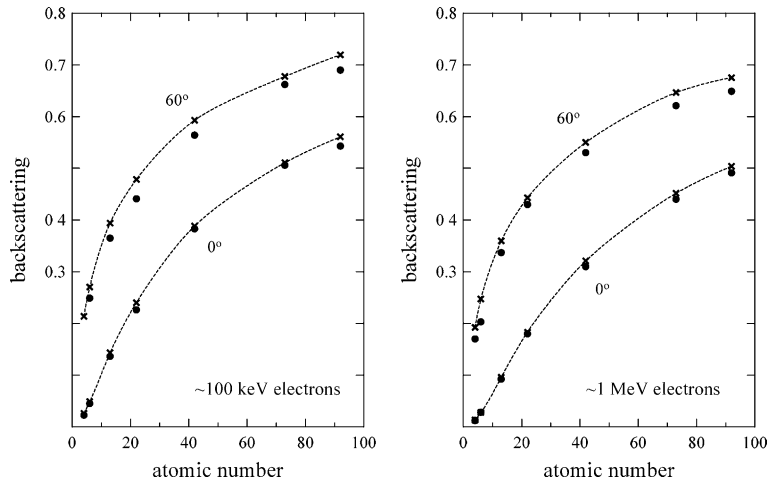


Fig. 4. Electron backscattering coefficients at two different energies and two angles of incidence (with respect to the normal to the sample surface) for bulk samples. Dots are experimental data from Lockwood et al. [43] and crosses, which have been joined by dashed curves for visual aid, are results from PENELOPE.

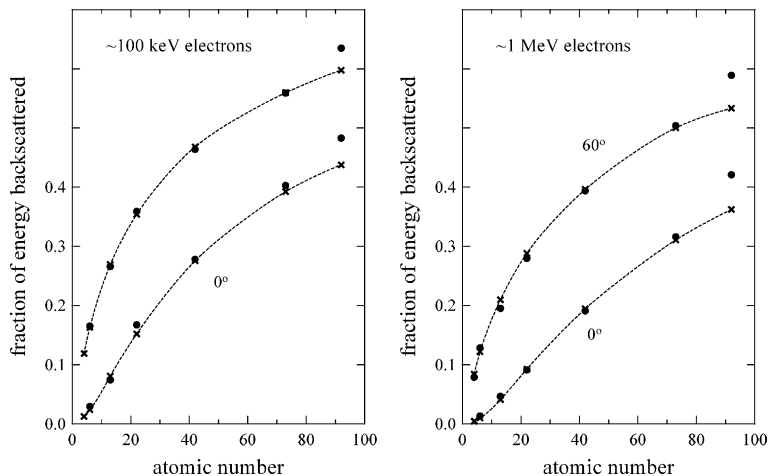


Fig. 5. Fraction of kinetic energy backscattered from semi-infinite samples when the incident beam has the indicated energy and impinges on the sample with the quoted angle relative to the surface normal. Details are the same as in Fig. 4.

DSMAX was given a very large value, which is equivalent to switching off the constraints imposed by this parameter.

In most of the simulations of group (iii), the probability that a primary electron produces a bremsstrahlung photon that reaches the “detector” is extremely low. In these cases, to achieve acceptably low statistical uncertainties with rea-

sonable computer times, we employed the variance-reduction technique known as interaction forcing (or mean free path scaling), as described by Salvat et al. [4]. Basically, this technique consists of artificially reducing the mean free path for the interaction of interest – bremsstrahlung emission in our case – and assigning to the emitted photons a weight less than unity to compensate for the

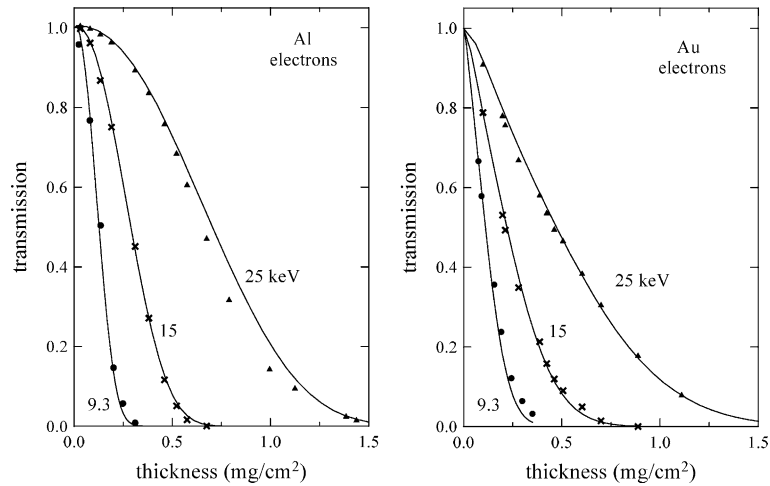


Fig. 6. Fractions of electrons transmitted through thin foils of aluminium and gold as functions of the foil thickness for three different beam energies at normal incidence. Lines represent results from PENELOPE, with a relative statistical uncertainty not larger than 0.001. Symbols are experimental data: dots are from [44] and crosses and triangles are from [45].

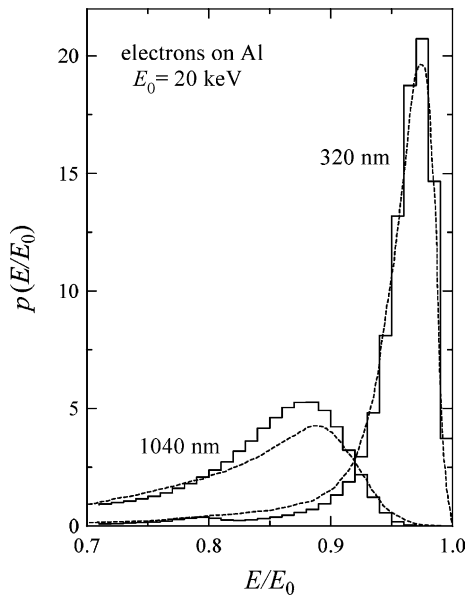


Fig. 7. Energy distributions of transmitted electrons impinging normally on two aluminium slabs of the indicated thicknesses; the electron beam energy E_0 was 20 keV. PENELOPE’s results are represented as histograms. Experimental data (dashed lines) are from [46].

increase in the probability of emission. The sub-routine package PENVARED.F, included in the PENELOPE distribution set, allows users to employ

interaction forcing as well as other variance-reduction techniques with minor modifications of their simulation main program.

All results reported in this work are per incident primary particle, usually an electron. The simulations were carried out on an Intel Pentium III processor at 733 MHz clock speed and with 256 MB of RAM. CPU timings varied amply, depending largely on the case. The simulation of showers generated by electrons with kinetic energies of 1 keV and 1 MeV in semi-infinite aluminium slabs took 1.17 and 12.8 ms per shower, respectively. For a 1 MeV electron beam on uranium, the generation of each shower took 55.1 ms. The statistical uncertainties (2σ) associated with the Monte Carlo distributions presented in this work are a few percent (normally 1–5%) of the maximum in the corresponding curve, except for several bremsstrahlung distributions, where statistical uncertainties reach some 10–15% of the maximum value.

Fig. 1 compares measured electron and positron backscattering coefficients (fractions of electrons and positrons backscattered from bulk samples) with simulated data. Primary particles were assumed to impinge normally on the target surface with a given energy. We may note the rather large fluctuations of the experimental data, which reflect

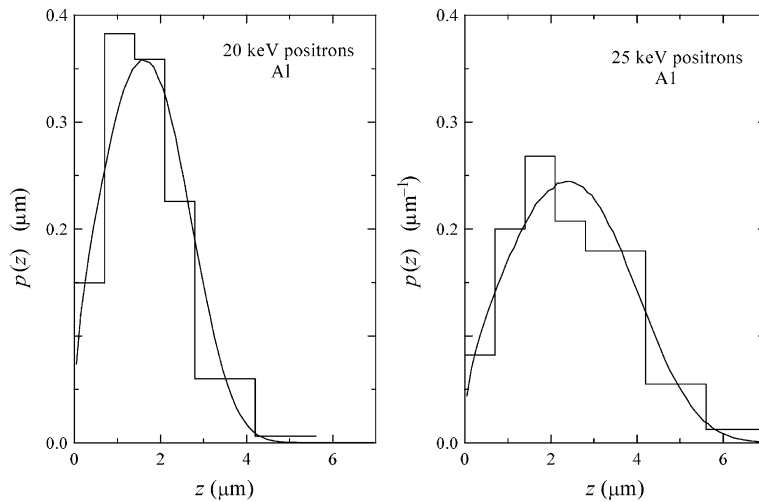


Fig. 8. Positron implantation profiles (i.e. depth-absorption profiles) in aluminium at the indicated beam energies and normal incidence. We display the probability distributions per *incident* (as opposed to absorbed) positron. The continuous curves are PENELOPE data. Histograms, representing the experimental measurements performed by Baker et al. [47] and reported in arbitrary units, were renormalized to the same area as the Monte Carlo calculations.

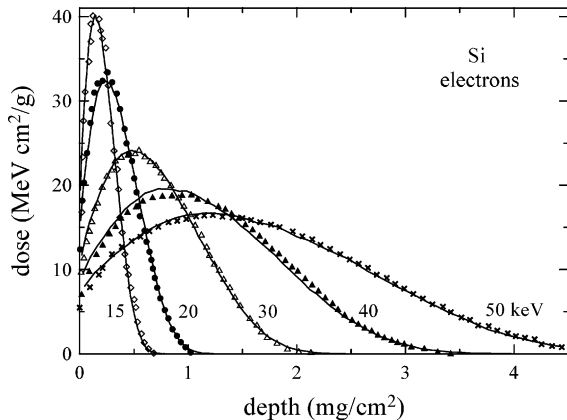


Fig. 9. Measured and simulated depth-dose distributions for electron beams with the indicated energies impinging normally on silicon. Lines are results from PENELOPE and symbols represent the measurements from [49].

the practical difficulties of the measurements associated with sample preparation, beam instabilities, etc. It is also worth mentioning that in most backscattering experiments the contribution from low-energy secondary electrons is suppressed by means of a bias potential of the order 50 V or so, which prevents electrons or positrons with kinetic energies below 50 eV from reaching the detector. Although many authors do not quote the exact

value of the bias potential used, the majority of electrons leave the target with energies larger than 100 eV and, therefore, the bias potential has only a small effect on the measured backscattering coefficient.

The differences between electrons and positrons are striking; they are mostly caused by corresponding differences between elastic scattering differential CSs for both particles. Electrons are attracted by the nucleus and interact more strongly than positrons, which are repelled by the nuclear charge, thus experiencing larger (on average) angular deflections which lead to a higher backscattering coefficient. We see that, for the energy range up to 100 keV, PENELOPE provides a description of the energy and atomic number dependence of the backscattering coefficients for electrons and positrons that is consistent with the body of available experimental data.

The electron backscattering fractions calculated with PENELOPE for MeV electrons are compared in Fig. 2 with an analytical expression proposed by Tabata et al. [40], which was obtained by least-squares fitting of a total of 1093 experimental data points collected in the energy region from 1 keV to 22 MeV. According to its authors, the uncertainty of the fit is estimated to be about 6%, which is

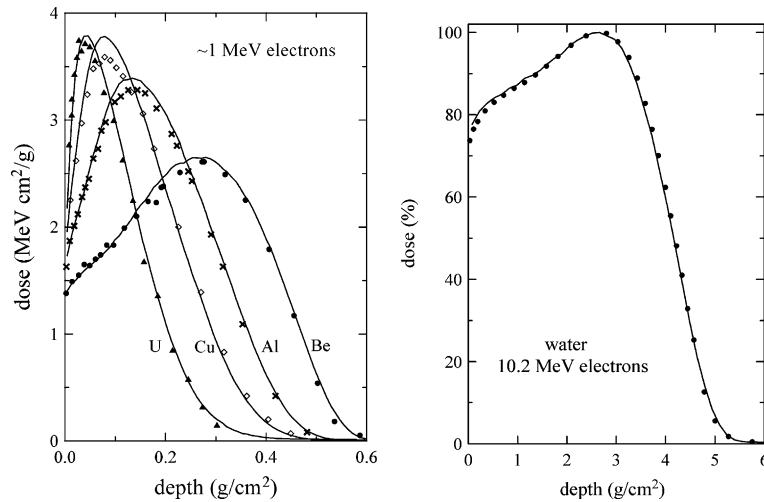


Fig. 10. Absorbed dose distributions for MeV electrons impinging on different materials. Left: depth-doses produced by 1 MeV electrons on copper and uranium and 1.033 MeV electrons on beryllium and aluminium. Right: central-axis absorbed dose produced by 10.2 MeV electrons on water. In all cases the lines represent results from PENELOPE. Experimental data were taken from the following sources: beryllium, aluminium, copper and uranium from [48]; water from [50].

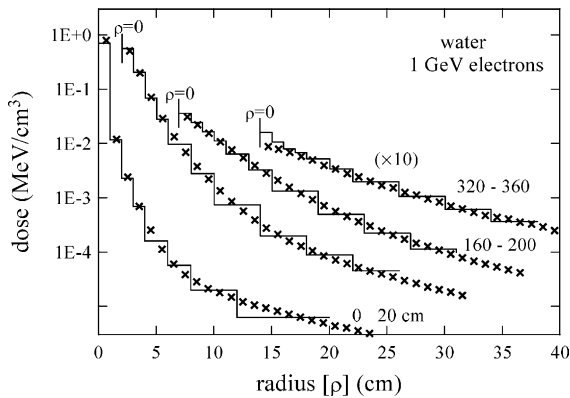


Fig. 11. Radial absorbed dose distribution in water for a 1 GeV electron pencil beam at normal incidence. Symbols are results from PENELOPE and the histograms are experimental data from [51]. Each curve represents the radial absorbed dose averaged over the indicated depth interval, in cm. The radial scale of deep layers is shifted and the deepest layer has also been scaled for clarity.

similar to the maximum deviation with respect to PENELOPE. In these simulations, $E_{\text{abs}}(e^-)$ was set equal to 0.05% of the beam energy. For the 200 keV beam in gold, which shows a larger departure from the analytical expression, this implies $E_{\text{ABS}}(e^-) = 100$ eV. If, instead, 1 keV is chosen, the resulting backscattering coefficient changes by

less than 1%, showing that the adopted value of EABS is fairly irrelevant, only provided it is small enough.

Fig. 3 shows energy distributions of electrons backscattered from various irradiated bulk samples. The simulated curves show a substantially larger low-energy contribution below some 10% of the initial beam energy and are otherwise in very good agreement with the experiment. This “absolute” agreement may be fortuitous, since the experimental data were normalized to the integrated backscattering fraction measured by Drescher et al. [30], which may be too low according to the present analysis (see also Fig. 1). Notice the large discrepancy at the low-energy end of the spectra, likely caused by the suppression of secondary electrons in the experiment. This observation had already been pointed out by Fernández-Varea et al. [41] using arguments based on the use of a different, more accurate in the low-energy domain, Monte Carlo code.

In Fig. 4 we compare backscattered fractions measured by Lockwood et al. [43] with simulation results for two different incident energies and impinging angles as a function of the atomic number. Results corresponding to the beam incident at 0° show excellent agreement with experiment,

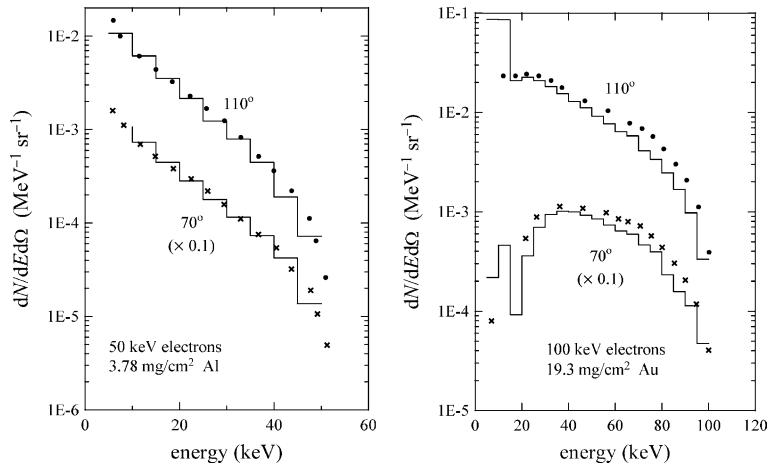


Fig. 12. Bremsstrahlung number spectra at two different angles relative to the direction of the incident electron beam. Electrons, with the indicated energies, impinged normally on the aluminium and gold foils of the indicated mass thicknesses. Histograms and symbols are simulation results from *PENELOPE* and experimental data from [52] (quoted in [53]), respectively. Notice that the curves corresponding to 70° have been scaled down for clarity.

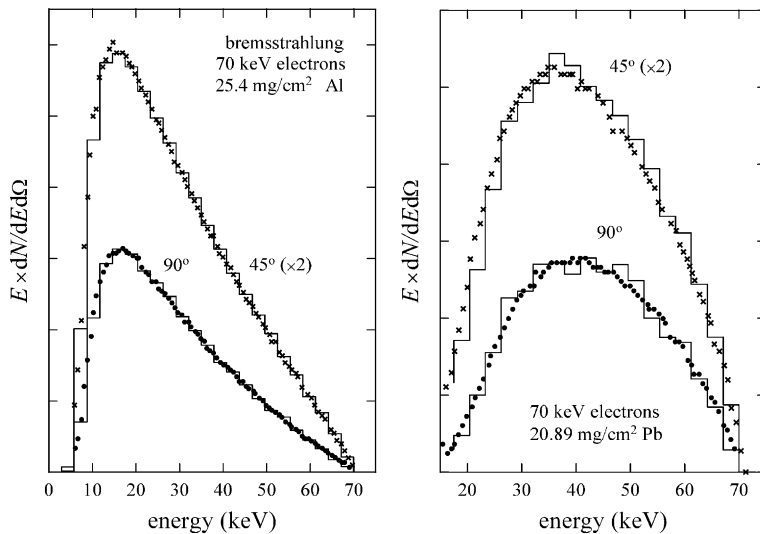


Fig. 13. Bremsstrahlung energy spectra, in arbitrary units, produced by a 70 keV electron beam on aluminium and lead slabs. Symbols are measurements from [54] and histograms are *PENELOPE* simulation results. The incident electron beams impinged on one of the surfaces of the target foil and the spectra were measured on the opposite face of the target, whose normal vector is \hat{n} . The beam impinged on the entrance face along a direction \hat{a} forming 45° with \hat{n} . The data labelled “ 45° ” (which have been scaled by a factor of 2 for clarity) were obtained along the direction \hat{n} . The other two sets of data represent photons emerging in a direction \hat{b} coplanar with \hat{a} and \hat{n} and perpendicular to \hat{a} .

whereas those of the beam at 60° present a slight but systematic (with respect to the atomic number) discrepancy. Fig. 5 compares the fraction of incident energy backscattered from the samples,

measured by the same authors, with the simulation, showing very good agreement at all energies, angles and atomic numbers, except for $Z = 92$. According to Lockwood and his co-workers, the

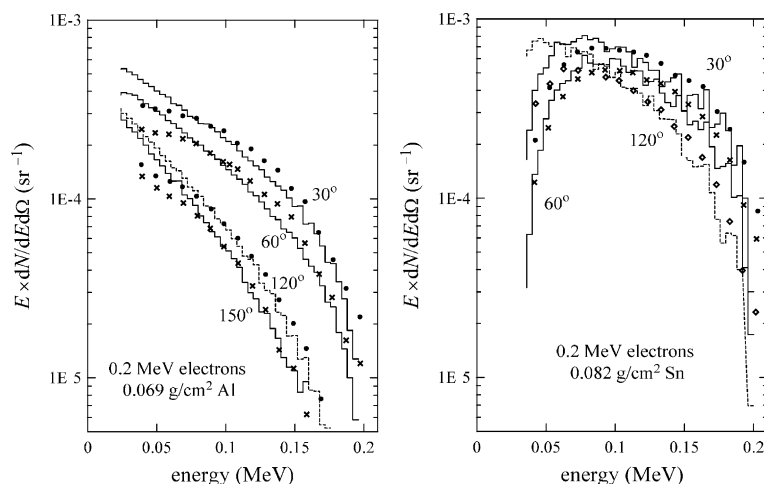


Fig. 14. Bremsstrahlung energy spectra for a 0.2 MeV electron beam incident on aluminium and tin foils of the indicated thicknesses. Symbols are experimental results from [55] and histograms are PENELOPE data. Electrons impinged normally and the spectra were obtained at the indicated angles with respect to the normal of the exit face of the sample.

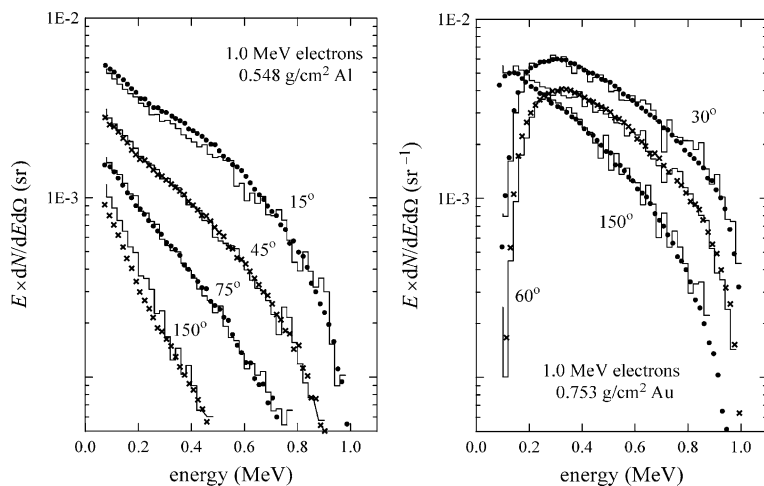


Fig. 15. Bremsstrahlung energy spectra for a 1 MeV electron beam. Details are the same as in Fig. 14.

analysis of these and other experimental data revealed strong evidence of a systematic error in the measurements on metallic uranium and, therefore, the disagreement in this last datum is deemed irrelevant.

Fig. 6 displays transmitted fractions of keV electron beams impinging normally on material slabs of different thicknesses. The overall agreement is remarkably good. Note the slight excess of electrons in aluminium at shallow depths due to

the knock-ons set in motion by the primary particle. The effect is not seen in gold because of its larger scattering power (i.e. smaller first transport mean free path), which prevents those secondaries from reaching the downstream side of the target.

Energy spectra of electrons transmitted through two thin aluminium foils of different thicknesses are presented in Fig. 7. Notice that the mean free paths for both elastic and inelastic collisions of electrons of 20 keV in this material are of the order

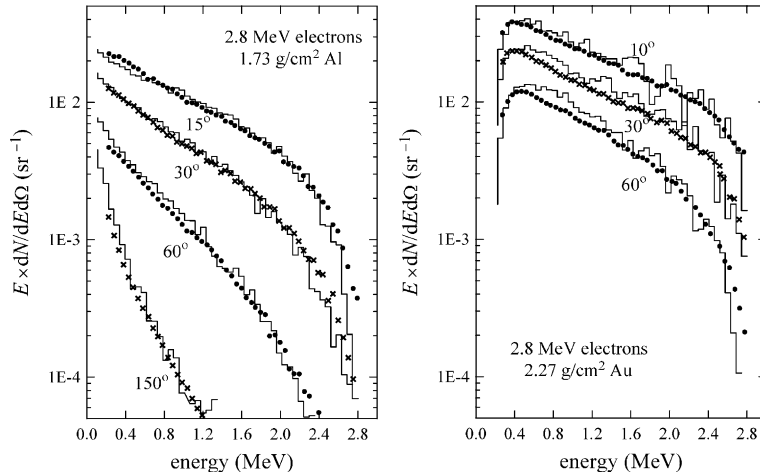


Fig. 16. Bremsstrahlung energy spectra for a 2.8 MeV electron beam. Details are the same as in Fig. 14.

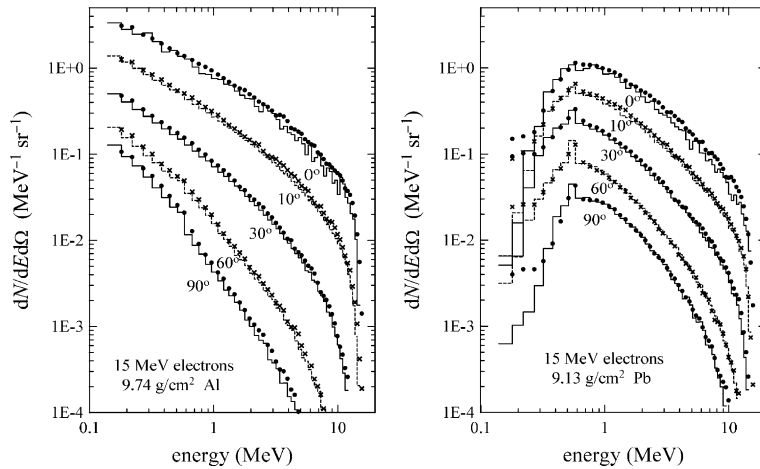


Fig. 17. Bremsstrahlung number spectra at different angles with the normal to the exit surface. A 15 MeV electron beam impinged normally on the aluminium and lead samples. Histograms are simulation results from PENELOPE and symbols represent measurements from [56]. Note the logarithmic scale on the energy axis.

of 20 nm and therefore this experiment involves only a few tens of interactions. A word of caution is in order here. The application of our simulation code to situations in which multiple scattering conditions are barely attained (i.e. when the number of hard and soft collisions is less than about 20) may occasionally give rise to some artifacts, such as the rising small bump at around $E/E_0 = 0.8$ for the thinnest foil and should therefore be used with care. It is also worth mentioning that the discrepancy around the maximum of the

curve corresponding to the thickest foil is also found when other Monte Carlo codes, more accurate in the low-energy regime, are used (see [41]).

Fig. 8 shows positron implantation profiles at moderately low beam energies. Although the experimental data are affected by considerably large uncertainties, as evidenced by the wide bins used, the general trends are clear and they are correctly reproduced by the simulation.

The results of group (ii) are shown in Figs. 9–11. Figs. 9 and 10 display depth–dose curves for

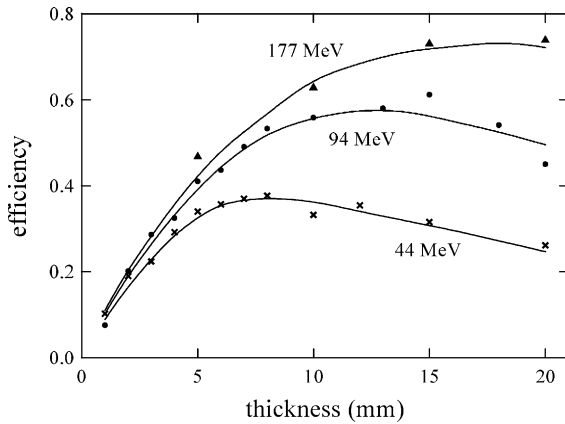


Fig. 18. Radiation converter efficiency as a function of the thickness of the lead layer for three photon energies. The experimental setup is described in the text. Symbols represent experimental measurements and the lines are cubic splines fit to the simulation results, which have an uncertainty not larger than 1%.

keV and MeV electron beams, respectively. The agreement between simulation and experiment is very good in the keV region, but some slight discrepancies do appear for copper and aluminium in the MeV case around the dose maximum. Simulation results obtained with the Monte Carlo code TIGER (one of the components of the ITS system [24]) and reported by Lockwood et al. [48] are in much closer agreement with PENELOPE than the experiment, therefore suggesting that the latter could have some hidden systematic error. Fig. 11 depicts the radial absorbed dose distribution produced by a 1 GeV electron pencil beam impinging normally on a water phantom. The close agreement found in this case supports our claim that PENELOPE is applicable at this high energy.

In the next group of figures two quantities are introduced. The first is the photon number spectrum, $\phi = dN/dE d\Omega$, representing the number of photons (N) per unit energy (E) and solid angle (Ω) intervals emerging from the sample in a given direction in space. The second quantity is the photon energy spectrum, defined as the product $E\phi$.

Fig. 12 shows photon number spectra for two different materials (intended to be representative of low and high atomic numbers), angles and energies. The experimental setup is described by Pla-

cius [52] and the actual data have been taken from Berger [53]. We have used the slab thicknesses stated in this latter work (and quoted in Fig. 12), which differ slightly from those in the original paper by Placious. The strong discrepancy for gold in the channels between 5 and 15 keV is due to the fact that characteristic X-ray lines were subtracted from the raw data by the experimentalists, whereas simulation results have not been altered to correct for this. According to Placious, the main source of error in processing his data was precisely originated by the subtraction of the L lines of gold, which have energies between 10 and 14 keV. The spectral shape in this region is further distorted by the abrupt change in the photon absorption due to the discontinuity of the photoelectric attenuation coefficient at the L edge. We would like to speculate whether the uncertainty introduced in the post-processing of the measurements could also contribute to the difference observed in the region between ~ 65 and 80 keV for gold, where the lines of the K series fall.

In Fig. 13, relative photon energy spectra for 70 keV electrons and two elements with very different atomic numbers are shown. Measurements and simulation results have been normalized to the same area, that is, radiation yield, above 15 keV. The reason for this truncation is to avoid the low-energy peak in the lead case. Although PENELOPE does generate characteristic X-rays resulting from inner-shell ionization by electron impact, electron inelastic collisions are described by means of a model that gives correct values of average quantities (such as the stopping power and the straggling parameter), but is not expected to describe inner-shell ionization faithfully.

Simulated and measured bremsstrahlung energy spectra for increasingly higher bombarding energies are presented in Figs. 14–16. Agreement is good, even though some differences do appear especially in the low-energy end of the spectra for the 200 keV case and in the 2.8 MeV gold case. The experimental uncertainty was estimated by the authors to be between 20–30% in the 200 keV cases, depending on the angle and of the order of 15–20% for the others.

Fig. 17 compares the simulated photon number spectra for a 15 MeV electron beam with the

experimental results reported by Faddegon et al. [56]. Agreement is excellent, except at the low-energy end of the lead case. According to Faddegon and his co-workers, the excessive number of photons in this region can be attributed to collimator effects, to scattering from objects near the target (two elements not described in our simulations) and also to charged-particle contamination.

Finally, Fig. 18 is the only case of group (iv). It displays the efficiency of a radiation converter as measured by Darriulat et al. [57] for photon energies of 44, 94 and 177 MeV. The converter consists of a lead foil, of variable thickness, on a 0.5-cm-thick layer of plastic scintillator. Photons impinged normally on the external surface of the lead foil; an event was counted as a conversion when the energy deposited on the scintillator exceeded 60 keV. In the simulations, following Nelson and Rogers [58], we have considered that the scintillator composition is that of the vinyltoluene-based plastic scintillator. The mechanism responsible for the increase of efficiency is the production of electron–positron pairs in lead. For larger thicknesses, the attenuation of the produced particles (and the subsequently emitted bremsstrahlung photons) in lead becomes more and more important and gives rise to the observed decrease in efficiency. Results from PENELOPE are seen to agree closely with experimental data.

7. Conclusion

The present set of benchmark comparisons of simulation results from PENELOPE with available experimental data confirms the reliability of the interaction models and tracking algorithms implemented in the simulation code in the energy range from a few keV up to 1 GeV. Overall, the agreement between simulation results and experimental values is excellent. A few discrepancies have been identified and attributed either to practical difficulties in setting up a “clean” experimental arrangement, to the post-processing of the raw experimental data or, not to be disregarded, to intrinsic inaccuracies or limitations of the interaction CSs used in PENELOPE. Work to obtain and implement more accurate CSs, particularly for

ionization of inner shells by electron impact, is in progress and will be presented elsewhere.

Acknowledgements

We would like to thank Mr. J. Asenjo for helping us to prepare some of the simulations. Financial support from the Fondo de Investigación Sanitaria of the Spanish Ministerio de Sanidad y Consumo, contract no. 01/0093, is gratefully acknowledged.

References

- [1] J. Sempau, E. Acosta, J. Baró, J.M. Fernández-Varea, F. Salvat, Nucl. Instr. and Meth. B 132 (1997) 377.
- [2] F. Salvat, J.M. Fernández-Varea, J. Baró, J. Sempau, Centro de Investigaciones Energéticas, Medioambientales y Tecnológicas Tech. Rep. 799, Madrid, 1996.
- [3] J. Baró, J. Sempau, J.M. Fernández-Varea, F. Salvat, Nucl. Instr. and Meth. B 100 (1995) 31.
- [4] F. Salvat, J.M. Fernández-Varea, E. Acosta, J. Sempau, PENELOPE – A Code System for Monte Carlo Simulation of Electron and Photon Transport, Nuclear Energy Agency OECD/NEA, Issy-les-Moulineaux, France, 2001, available in pdf format on the web at <http://www.nea.fr>.
- [5] ISO, Guide to the Expression of Uncertainty in Measurement, International Organization for Standardization, Genève, Switzerland, 1995.
- [6] J. Baró, M. Roteta, J.M. Fernández-Varea, F. Salvat, Radiat. Phys. Chem. 44 (1994) 531.
- [7] D. Brusa, G. Stutz, J.A. Riveros, J.M. Fernández-Varea, F. Salvat, Nucl. Instr. and Meth. A 379 (1996) 167.
- [8] D.E. Cullen, J.H. Hubbell, L. Kissel, Lawrence Livermore National Laboratory Tech. Rep. UCRL-50400, Vol. 6, Rev. 5, Livermore, CA, 1997.
- [9] S.T. Perkins, D.E. Cullen, M.H. Chen, J.H. Hubbell, J. Rathkopf, J. Scofield, Lawrence Livermore National Laboratory Tech. Rep. UCRL-50400, Vol. 30, Livermore, CA, 1991.
- [10] F. Salvat, R. Mayol, Comput. Phys. Commun. 74 (1993) 358.
- [11] J.M. Fernández-Varea, R. Mayol, J. Baró, F. Salvat, Nucl. Instr. and Meth. B 73 (1993) 447.
- [12] F. Salvat, J.M. Fernández-Varea, Nucl. Instr. and Meth. B 63 (1992) 255.
- [13] D. Liljequist, J. Phys. D: Appl. Phys. 16 (1983) 1567.
- [14] R.M. Sternheimer, Phys. Rev. 88 (1952) 851.
- [15] ICRU Tech. Rep. 37, Bethesda MD, 1984.
- [16] S. Segui, M. Dingfelder, F. Salvat, private communication.
- [17] X. Llovet, C. Merlet, F. Salvat, J. Phys. B: At. Mol. Opt. Phys. 35 (2002) 973.

- [18] H.W. Koch, J.W. Motz, *Rev. Mod. Phys.* 31 (1959) 920.
- [19] Y.-S. Tsai, *Rev. Mod. Phys.* 46 (1974) 815, Erratum: 49 (1977) 421.
- [20] S.M. Seltzer, M.J. Berger, *Nucl. Instr. and Meth. B* 12 (1985) 95.
- [21] S.M. Seltzer, M.J. Berger, *At. Data Nucl. Data Tables* 35 (1986) 345.
- [22] L. Kissel, C.A. Quarles, R.H. Pratt, *At. Data Nucl. Data Tables* 28 (1983) 381.
- [23] W.R. Nelson, H. Hirayama, D.W.O. Rogers, Stanford Linear Accelerator Center Tech. Rep. SLAC-265, Stanford, CA, 1985.
- [24] J.A. Halbleib, R.P. Kensek, T.A. Mehlhorn, G.D. Valdez, S.M. Seltzer, M.J. Berger, Sandia National Laboratories Tech. Rep. SAND91-1634, Albuquerque, NM, 1992.
- [25] J.F. Briesmeister, Los Alamos National Laboratory Tech. Rep. LA-12625-M Version 4B, Los Alamos, NM, 1997.
- [26] E. Acosta, X. Llovet, F. Salvat, *Appl. Phys. Lett.* 80 (2002) 3228.
- [27] W. Heitler, *The Quantum Theory of Radiation*, Oxford University Press, London, 1954.
- [28] M.J. Berger, in: B. Alder, S. Fernbach, M. Rotenberg (Eds.), *Methods in Computational Physics*, Vol. 1, Academic Press, New York, 1963, p. 135.
- [29] E.R. Woodcock, T. Murphy, P.J. Hemmings, S.C. Longworth, in: *Proceedings of the Conference on Applications of Computing Methods to Reactor Problems*, 1965, p. 557.
- [30] H. Drescher, L. Reimer, H. Seidel, *Z. Angew. Phys.* 29 (1970) 331.
- [31] G. Neubert, S. Rogaschewski, *Phys. Stat. Sol. (a)* 59 (1980) 35.
- [32] H.-J. Fitting, *Phys. Stat. Sol. (a)* 26 (1974) 525.
- [33] H.-J. Hunger, L. Küchler, *Phys. Stat. Sol. (a)* 56 (1979) K45.
- [34] J. Schou, H. Sørensen, *J. Appl. Phys.* 49 (1978) 816.
- [35] V.E. Cosslett, R.N. Thomas, *Brit. J. Appl. Phys.* 16 (1965) 779.
- [36] H.E. Bishop, in: P. Deschamps, J. Philibert, R. Castaing (Eds.), *Optique des rayons X et microanalyse*, Hermann, Paris, 1966, p. 153.
- [37] G.R. Massoumi, N. Hozhabri, W.N. Lennard, P.J. Schultz, *Phys. Rev. B* 44 (1991) 3486.
- [38] P.G. Coleman, L. Albrecht, K.O. Jensen, A.B. Walker, *J. Phys.: Condens. Matter* 4 (1992) 10311.
- [39] J. Mäkinen, S. Palko, J. Martikainen, P. Hautojärvi, *J. Phys.: Condens. Matter* 4 (1992) L503.
- [40] T. Tabata, P. Andreo, K. Shinoda, *Radiat. Phys. Chem.* 54 (1999) 11.
- [41] J.M. Fernández-Varea, D. Liljequist, S. Csillag, R. Rätty, F. Salvat, *Nucl. Instr. and Meth. B* 108 (1996) 35.
- [42] E.H. Darlington, *J. Phys. D: Appl. Phys.* 8 (1975) 85.
- [43] G.J. Lockwood, G.H. Miller, J.A. Halbleib, Sandia Laboratories Tech. Rep. SAND80-1968, Albuquerque, NM, 1981.
- [44] L. Reimer, H. Drescher, *J. Phys. D: Appl. Phys.* 10 (1977) 805.
- [45] G. Neubert, S. Rogaschewski, *J. Phys. D: Appl. Phys.* 17 (1984) 2439.
- [46] R. Shimizu, Y. Kataoka, T. Ikuta, T. Koshikawa, H. Hashimoto, *J. Phys. D: Appl. Phys.* 9 (1976) 101.
- [47] J.A. Baker, N.B. Chilton, P.G. Coleman, *Appl. Phys. Lett.* 59 (1991) 164.
- [48] G.J. Lockwood, L.E. Ruggles, G.H. Miller, J.A. Halbleib, Sandia Laboratories Tech. Rep. SAND79-0414, Albuquerque, NM, 1980.
- [49] U. Werner, F. Koch, G. Oelgart, *J. Phys. D: Appl. Phys.* 21 (1988) 116.
- [50] A. Brahme, G. Hultén, H. Svensson, *Phys. Med. Biol.* 20 (1975) 39.
- [51] C.J. Crannell, H. Crannell, R.R. Whitney, H.D. Zeman, *Phys. Rev.* 184 (1969) 426.
- [52] R.C. Placious, *J. Appl. Phys.* 38 (1967) 2030.
- [53] M.J. Berger, in: T.M. Jenkins, W.R. Nelson, A. Rindi (Eds.), *Monte Carlo Transport of Electrons and Photons*, Plenum Press, New York, 1988, p. 183.
- [54] R. Ambrose, D.L. Kahler, H.E. Lehtihet, C.A. Quarles, *Nucl. Instr. and Meth. B* 56–57 (1991) 327.
- [55] D.H. Rester, W.E. Dance, J.H. Derrickson, *J. Appl. Phys.* 41 (1970) 2682.
- [56] B.A. Faddegon, C.K. Ross, D.W.O. Rogers, *Med. Phys.* 18 (1991) 727.
- [57] P. Darriulat, E. Cygi, M. Holder, K. McDonald, H. Pugh, F. Schneider, K. Tittel, *Nucl. Instr. and Meth.* 129 (1975) 105.
- [58] W.R. Nelson, D.W.O. Rogers, in: T.M. Jenkins, W.R. Nelson, A. Rindi, A.E. Nahum, D.W.O. Rogers (Eds.), *Monte Carlo Transport of Electrons and Photons*, Plenum Press, New York, 1988, p. 287.